

Graphene Nanoribbons from Tetraphenylethene-Based Polymeric Precursor: Chemical Synthesis and Application in Thin-Film Field-Effect Transistor

Ji Ma,^a Haoyun Zhu,^a Wei Huang,^a Tingting Lin,^b Xiaoyong Pan,^b and Weizhi Wang^{*a}

^a State Key Laboratory of Molecular Engineering of Polymers, Collaborative Innovation Center of Polymers and Polymer Composite Materials, Department of Macromolecular Science, Fudan University, Shanghai 200433, China

^b Institute of Materials Research and Engineering, A*STAR (Agency for Science, Technology and Research), 2 Fusionopolis Way, Innovis, #08-03, Singapore 138634, Singapore

Graphene nanoribbons (GNRs) with a non-zero bandgap are regarded as a promising candidate for the fabrication of electronic devices. In this study, large-scale solution synthesis of narrow GNRs was firstly achieved by the intramolecular cyclodehydrogenation of kinked tetraphenylethene (TPE) polymer precursors prepared by A_2B_2 -type Suzuki-Miyaura polymerization. After the cyclization reaction, the nanoribbons have a better conjugation than the twisted polymer precursor, resulting in obvious red shift in UV/vis absorption and photoluminescence (PL) spectra. The efficient formation of conjugated nanoribbons was also investigated by Raman, FTIR spectroscopy, and microscopic studies. Furthermore, such structurally well-defined GNRs have been successfully developed for top-gated field-effect transistor (FET) by directly solution processing. The AFM images show that the prepared-GNRs thin films form crystalline fibrillar intercalating networks, which can effectively facilitate the charge transport. These FET devices with ion-gel gate dielectrics exhibit low-voltage operation (<5 V) with excellent mobility up to $0.41 \text{ cm}^2 \cdot \text{V}^{-1} \cdot \text{s}^{-1}$ and an on-off ratio of 3×10^4 , thus opening up new opportunities for flexible GNRs-based electronic devices.

Keywords graphene, nanoribbons, transistor, tetraphenylethene, device

Introduction

Graphene nanoribbons (GNRs), confined and long strips of graphene, are attracting the widespread attention of researchers in chemistry, physics, and materials owing to their interesting optoelectronic properties and potential electronic applications.^[1-4] Great effort has been dedicated to creating high-quality GNRs in recent years. Various top-down techniques, such as cutting of graphene on a surface,^[5,6] sonochemical extraction from expanded graphite,^[7,8] and unzipping of carbon nanotubes were used to tailor GNRs.^[9-12] However, these methods lacked size and edge control of GNRs, which critically undermines their electronic properties and hinders their practical applications in electronic devices. In contrast, bottom-up chemical synthesis approaches: decomposition of molecules inside carbon nanotubes,^[13,14] surface-assisted cyclodehydrogenation reactions,^[15-17] and chemical vapor deposition from one-dimensional templates,^[18-21] can produce structurally perfect GNRs with uniform lateral structures. Nevertheless, these bottom-up methods are inefficient and the

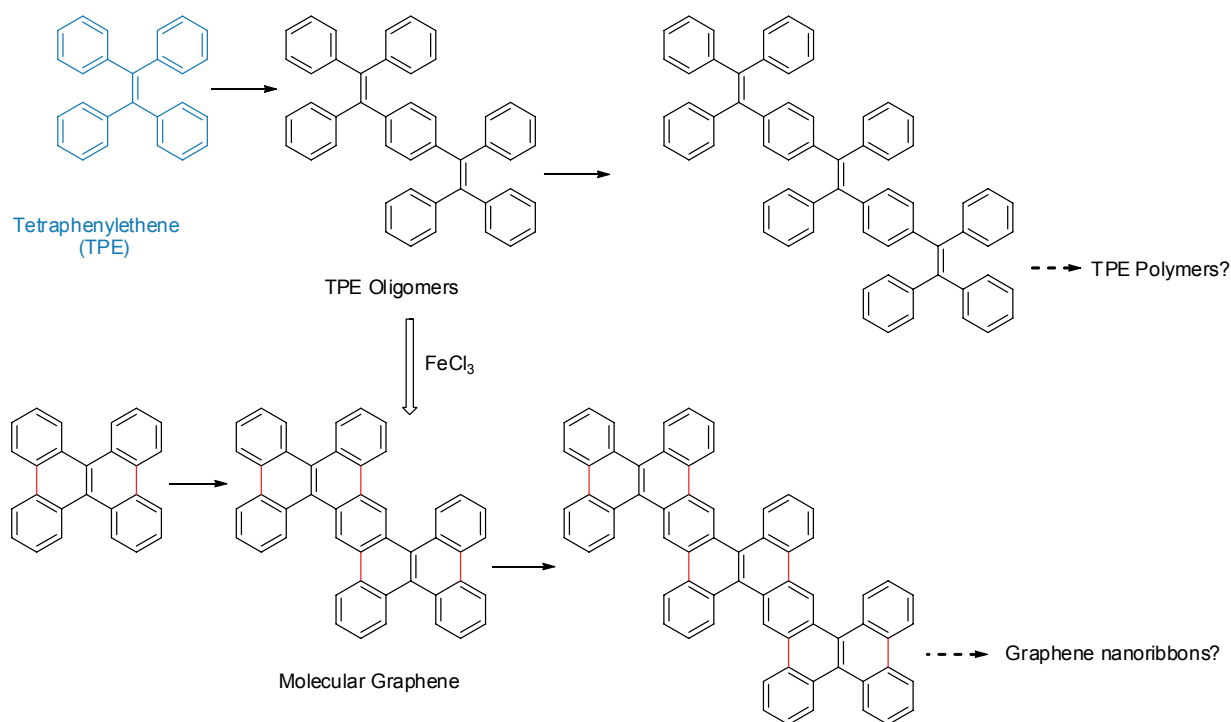
quantities are very small. Currently, a novel bottom-up solution-mediated synthesis method has been developed to yield large quantities of GNRs with different conformation. Furthermore, this method can conveniently transfer the resulting GNRs onto dielectric surfaces for the fabrication of field-effect transistor (FET) devices.^[22-26]

In general, the bottom-up solution-mediated synthesis of GNRs involves three key steps: (1) design of the appropriate molecular precursors; (2) solution polymerization of the molecular precursors; (3) graphitization of the resulting polymers via Scholl reaction.^[22-24,27,28] To the best of our knowledge, the studies on polymer precursors for GNRs mainly focus on polyphenylene till now. This may restrict the diversity of GNRs such as different aspect ratios and edge structures. Therefore, exploring other novel types of polymer precursors is very important. Our previous studies have proven that tetraphenylethenes (TPE) (Scheme 1),^[29,30] which are easier to synthesize and derive, can be used as good precursors to obtain the molecular graphene through a

* E-mail: weizhiwang@fudan.edu.cn; Tel.: 0086-021-65643836

Received September 17, 2015; accepted October 26, 2015; published online December 15, 2015.

Supporting information for this article is available on the WWW under <http://dx.doi.org/10.1002/cjoc.201500672> or from the author.

Scheme 1 Schematic overview of the bottom-up synthesis of molecular graphene from tetraphenylethene precursors

facile and highly efficient cyclization reaction using iron(III) chloride (FeCl_3) as an oxidant.^[31] Inspired by this study, we further explored the possibility of synthesizing structurally defined GNRs from TPE polymers through the Scholl reaction. Herein, we demonstrated that large quantities of GNRs with atomically precise structure can also be produced by intramolecular cyclodehydrogenation of the tailor-made tetraphenylthene polymer (PTPE) precursor using Scholl reaction. Then we used this synthesized GNRs as the active layers to fabricate thin film FET devices by directly solution processing. These devices can work well at low gate voltage and exhibit a typical p-type transport behavior with an excellent charge carrier mobility and high on-off ratio.

Experimental

General methods

^1H and ^{13}C NMR spectra were measured on Varian Mercury Plus 400 spectrometer in deuterated chloroform (CDCl_3) or dichloromethane (CD_2Cl_2) and chemical shifts were reported with tetramethylsilane (TMS) as an internal standard. Matrix assisted laser desorption time of flight mass spectrometry (MALDI-TOF) measurement was carried out on the AB SCIEX TOF/TOF™ 5800 Analyzer (AB Sciex, Framingham, MA, USA). Elemental analysis was performed on a VARIO EL3 instrument (ELEMENTAR, Germany). Gel permeation chromatography (GPC) was performed on an Agilent 1100 with a G1310A pump, a G1310A refractive-index

detector, and a G1314A variable-wavelength detector with THF as the eluent at a flow rate of 1.0 mL/min at 35 °C using standard polystyrene (PS) for universal calibration. UV/Vis absorption spectra (UV) were obtained on a Shimadzu UV-3150 spectrophotometer. The absorption onset point is determined by the threshold point of UV curve. Fluorescence spectra (PL) were measured on a Shimadzu RF-5310 PC fluorometer at room temperature. Cyclic voltammetry (CV) was carried out on a T30/ FRA2 electrochemical workstation. CV measurements of the oligomer films coated on a glassy carbon electrode (0.08 cm^2) were performed in an electrolyte of 0.1 mol/L tetrabutylammonium hexafluorophosphate (TBAPF_6) in acetonitrile using ferrocene (FOC) (4.8 eV under vacuum) as the internal standard at a scan rate of $50\text{ mV}\cdot\text{s}^{-1}$ at room temperature under the protection of argon. The counter electrode was a platinum wire and an Ag/AgNO_3 electrode was used as the reference electrode. Thermogravimetric analysis (TGA) was conducted with a PerkinElmer Pyris 1 TGA under a nitrogen atmosphere and differential scanning calorimetry analysis (DSC) was performed with a Q2000 DSC (TA Instruments LLC). The infrared spectra were measured on a Nicolet 6700 FT-IR spectrometer from ThermoElectron Corporation. Raman spectrum was recorded using an XploRA™ Raman microscope (LabRam, Horiba, Jobin-Yvon, France) with a 532 nm laser. Powder X-ray diffraction (XRD) patterns were conducted on an X'Pert-Pro MPD diffractometer with $\text{Cu K}\alpha$ radiation ($\lambda = 1.5418\text{ \AA}$) at 25 °C. Atomic force microscopy studies were performed with a Digital

Instruments NanoScope IV (Bruker Multimode 8, America) operating in the tapping mode. Polarizing microscope images were obtained using DM2500P. Scanning electron microscope (SEM) images were examined by TESCAN VEGA TS 5136MM. Scanning tunneling microscopy (STM) was carried out with Nanoscope IIIa instrument at the solid/liquid interface in 1-phenyloctane at room temperature [0.1 mmol/L toluene solution on freshly cleaved highly oriented pyrolytic graphite (HOPG)]. A mechanically etched Pt/Ir (90 : 10) wire was used as the STM tip. The instrument was operated in constant current mode at a tunnelling current of 319 pA and a bias voltage of 610 mV. X-ray crystallographic data were collected on a P4 Bruker diffractometer equipped with a Bruker SMART 1K CCD area detector (employing the program SMART) and a rotating anode utilizing graphite-monochromated Mo K α radiation ($\lambda = 0.71073$ Å). Data processing was carried out by use of the program SAINT, while the program SADABS was utilized for the scaling of diffraction data, the application of a decay correction and an empirical absorption correction based on redundant reflections. The structures were solved by using the direct-methods procedure in the Bruker SHELXL program library and refined by full-matrix least-squares methods on F2. All non-hydrogen atoms were refined using anisotropic thermal parameters, and hydrogen atoms were added as fixed contributors at calculated positions, with isotropic thermal parameters based on the carbon atom to which they are bonded.

FET device fabrication

Some commercially available (300-nm-thick SiO₂/p++ Si) substrates were washed with acetone and methanol, H₂O₂/H₂SO₄ and deionized water in turn. The GNRs **6** in toluene solutions (2 mg/mL) were spin-coated on these clean SiO₂/Si wafers at the rotating speed of 6500 r/min. The obtained thin films were thermally annealing at 150 °C for 20 min in a vacuum environment. Then, 50-nm-thick gold (Au) source and drain electrodes (the typical channel length and width are both 1000 μ m) were vapor-deposited on the GNRs thin films. For ion gel gate dielectric formation, poly(styrene-block-methyl methacrylate-block styrene) (PS-PMMA-PS; $M_{PS} = 4.3$ kg/mol, $M_{PMMA} = 12.5$ kg/mol, $M_w = 21.1$ kg/mol) triblock copolymer and 1-ethyl-3-methylimidazolium bis(trifluoromethylsulfonyl) imide ionic liquid were dissolved in ethyl propionate solution at a 0.7 : 9.3 : 20 ratio (w/w) and then drop-cast to cover the surfaces of the GNRs films with an Au drain and source contact. After the solvent was removed, an ion gel film was formed. After that, the transistor channels were covered with a thin aluminum foil (thickness of 0.03 mm) to form the top-gate electrode. The transistor characteristics were measured using a semiconductor parameter analyzer (Keithley 4200, Keithley Co.) at room temperature in approxi-

mately 10⁻⁵ Pa vacuum. The average values of the FET mobility were obtained for at least 15 devices.

Synthetic details

Chemicals and reagents were purchased from Aldrich or Acros Chemical Co. unless specifically stated. Tetrahydrofuran (THF) and toluene were distilled under nitrogen from sodium benzophenone ketyl immediately prior to use. All other solvents were of analytical grade and were purified using standard methods.

(E)-1,2-Dibromo-1,2-diphenylethene (1) 6 g of diphenylacetylene (1.0 equiv., 33.7 mmol) was dissolved in dichloromethane (60 mL) in a flask, into which 5.86 g of bromine (1.1 equiv., 37.1 mmol) was added dropwise. After stirring for 0.5 h at room temperature, the reaction mixture was washed with saturated aqueous solution of sodium hydrogen sulfite. The organic layer was separated and dried over magnesium sulfate and then evaporated to dryness. The crude product was purified by recrystallization from ethanol to afford a white crystal in 85% yield. The obtained crystal was characterized crystallographically, which confirmed its expected *trans*-configuration structure. ¹H NMR (400 MHz, CDCl₃) δ : 7.57–7.51 (m, 4H), 7.46–7.37 (m, 6H); ¹³C NMR (100 MHz, CDCl₃) δ : 140.76, 129.08, 128.92, 128.38, 118.06. Anal. calcd for C₁₂H₁₀Br₂: C 49.74, H 2.98, Br 47.28; found C 49.82, H 2.96.

(4-Bromophenyl)(4-*tert*-butylphenyl)methanone (2) To a stirred slurry of 5.32 g (0.04 mol) of aluminum chloride and 2.68 g of *tert*-butylbenzene (0.02 mol) in 30 mL of CS₂ was added dropwise a solution of 4.34 g (0.02 mol) of *p*-bromobenzoyl chloride in 8 mL of CS₂ at room temperature. After that, water was cautiously added to the mixture on an ice bath. The reaction mixture was extracted by dichloromethane. The organic layer was washed with sodium hydroxide and dried with magnesium sulfate. The solvent was then removed by rotary evaporation to yield a white solid (4.80 g, 76%). Single crystal of **2** was isolated from their dichloromethane solution, and was characterized crystallographically. ¹H NMR (400 MHz, CDCl₃) δ : 7.74–7.49 (m, 8H), 1.37 (s, 9H); ¹³C NMR (100 MHz, CDCl₃) δ : 195.34, 156.52, 136.64, 134.38, 131.53, 131.50, 130.02, 127.21, 125.38, 35.16, 31.13. Anal. calcd for C₁₇H₁₇BrO: C 64.37, H 5.40, Br 25.19, O 5.04; found C 64.32, H 5.46.

(Z)-1,2-Bis(4-bromophenyl)-1,2-bis(4-*tert*-butylphenyl)ethane (3) A flask equipped with a magnetic stirrer was charged with zinc dust (1.56 g, 24 mmol) and 50 mL THF under nitrogen atmosphere. The mixture was cooled to 0 °C, and titanium tetrachloride (2.30 g, 12 mmol) was added slowly with a syringe. The mixture was refluxed for 2 h and cooled to 0 °C. Compound **2** (3.16 g, 10 mmol) in THF (30 mL) was added to the mixture. Then the mixture was refluxed until TLC showed complete conversion. When cooled, the reaction was stopped by adding saturated aqueous NH₄Cl solu-

tion. The organic layer was extracted by dichloromethane and dried by magnesium sulfate for 30 min. Dried organic layer was concentrated by rotary evaporation. Finally, the resulting white residue (two isomers) was obtained. Then, the *Z*-isomers of **3** were separated from their *n*-hexane/dichloromethane solutions (*V/V*, 1/5) by slow evaporation at room temperature, and its configuration was confirmed by X-ray crystallographic analysis. As shown in Figure S1, the *Z*-isomers **3** was suspended in the upper layer of the solution, however, the *E*-isomers **3'** precipitated in the bottom of glass tube. Finally, needle crystals of *Z*-isomer **3** were obtained in 65% yield (0.97 g). ¹H NMR (400 MHz, CDCl₃) δ: 7.24 (d, *J*=8.6 Hz, 4H), 7.07 (d, *J*=8.6 Hz, 4H), 6.91–6.84 (m, 8H), 1.24 (s, 18H); ¹³C NMR (100 MHz, CDCl₃) δ: 149.63, 142.59, 140.01, 139.87, 132.99, 130.71, 124.75, 124.47, 120.49, 34.43, 31.24. MS (MALDI-TOF) *m/z* (%): 602.08 (13) [M⁺], 524.17 (40) [M–Br]⁺, 444.26 (100) [M–2Br]⁺ (calcd C₃₄H₃₄Br₂=602.44). Anal. calcd for C₃₄H₃₄Br₂: C 67.78, H 5.69, Br 26.53; found C 67.68, H 5.72.

(Z)1,2-Bis(4-(4,4,5,5-tetramethyl-1,3,2-dioxaborolan-2-yl)phenyl)-1,2-bis(4-*tert*-butylphenyl)ethane (4) A mixture of compound **3** (1.80 g, 3 mmol), bis(pinacolato)diboron (1.52 g, 6 mmol), potassium acetate (1.96 g, 20 mmol), Pd(dppf)Cl₂ (0.07 g, 0.1 mmol) in anhydrous 1,4-dioxane (50 mL) was refluxed under argon for 12 h, and then water (10 mL) was added. The crude product was extracted into ethyl acetate, washed with water, and dried over anhydrous sodium sulfate. After removing solvent under reduced pressure, the residue was purified by column chromatography using petroleum ether/ethyl acetate (10 : 1, *V/V*) as eluent. A white powder of **4** was obtained in the yield of 63.4% (1.32 g). Single crystals of compound **4** were isolated from the dichloromethane (DCM)/methanol solution, and its configuration was confirmed by X-ray crystallographic analysis. ¹H NMR (400 MHz, CDCl₃) δ: 7.52 (d, *J*=8.3 Hz 4H), 7.06–7.03 (m, 8H), 6.86 (d, *J*=8.6 Hz, 4H), 1.32 (s, 24H), 1.23 (s, 18H); ¹³C NMR (100 MHz, CDCl₃) δ: 149.19, 146.88, 140.87, 140.61, 134.06, 130.86, 130.73, 124.27, 83.63, 34.37, 31.26, 24.90. MS (MALDI-TOF) *m/z* (%): 696.32 (100) [M⁺] (calcd C₄₆H₅₈B₂O₄=696.57). Anal. calcd for C₄₆H₅₈B₂O₄: C 79.32, H 8.39, B 3.10, O 9.19; found C 79.32, H 8.42.

Tetraphenylethene polymer precursor (5) In a 25 mL Schlenk tube, a mixture of monomer **1** (336 mg, 1 mmol), monomer **4** (696 mg, 1 mmol), K₂CO₃ (2 M/H₂O, 3 mL, 6 mmol) and Aliquat 336 (0.015 mmol) in 10 mL of toluene was degassed with an argon stream for 15 min. Pd(PPh₃)₄ (62 mg, 0.05 mmol) was added quickly and the reaction mixture was degassed three times via 'freeze-pump-thaw' cycles. The reaction was refluxed under argon and stirred for 3 d. The polymers were endcapped with bromobenzene and phenylboronic acid pinacol ester by successively adding a degassed solution (0.2 mL of 0.01 mol·L⁻¹ toluene) via a syringe and the reaction was refluxed for another 12 h. The so-

lution was cooled to room temperature and poured into methanol. The precipitate was filtered and the polymers were then Soxhlet extracted with acetone for 3 d. The residue was redissolved in hot THF and precipitated again into methanol. The solid was filtered, washed with methanol and dried in vacuum to give polymer **5** as a slightly gray solid (450 mg, Yield=73%). GPC analysis: *M_n*=0.79×10⁴ g/mol, *M_w*=1.05×10⁴ g/mol, and PDI=1.33 (against PS standard). ¹H NMR (400 MHz, CD₂Cl₂) δ: 7.61–7.25 (m, 4H), 7.23–6.65 (m, 16H), 1.39–0.94 (m, 14H); ¹³C NMR (100 MHz, CD₂Cl₂) δ: 149.35, 131.69, 131.18, 130.80, 127.59, 125.67, 124.40, 109.99, 34.27, 30.98, 29.67; FT IR *v*: 3082, 3057, 3027, 2961, 2921, 2902, 2861, 1606, 1501, 1464, 1396, 1258, 1201, 1104, 1016, 866, 838, 823, 802, 761, 699, 628 cm⁻¹.

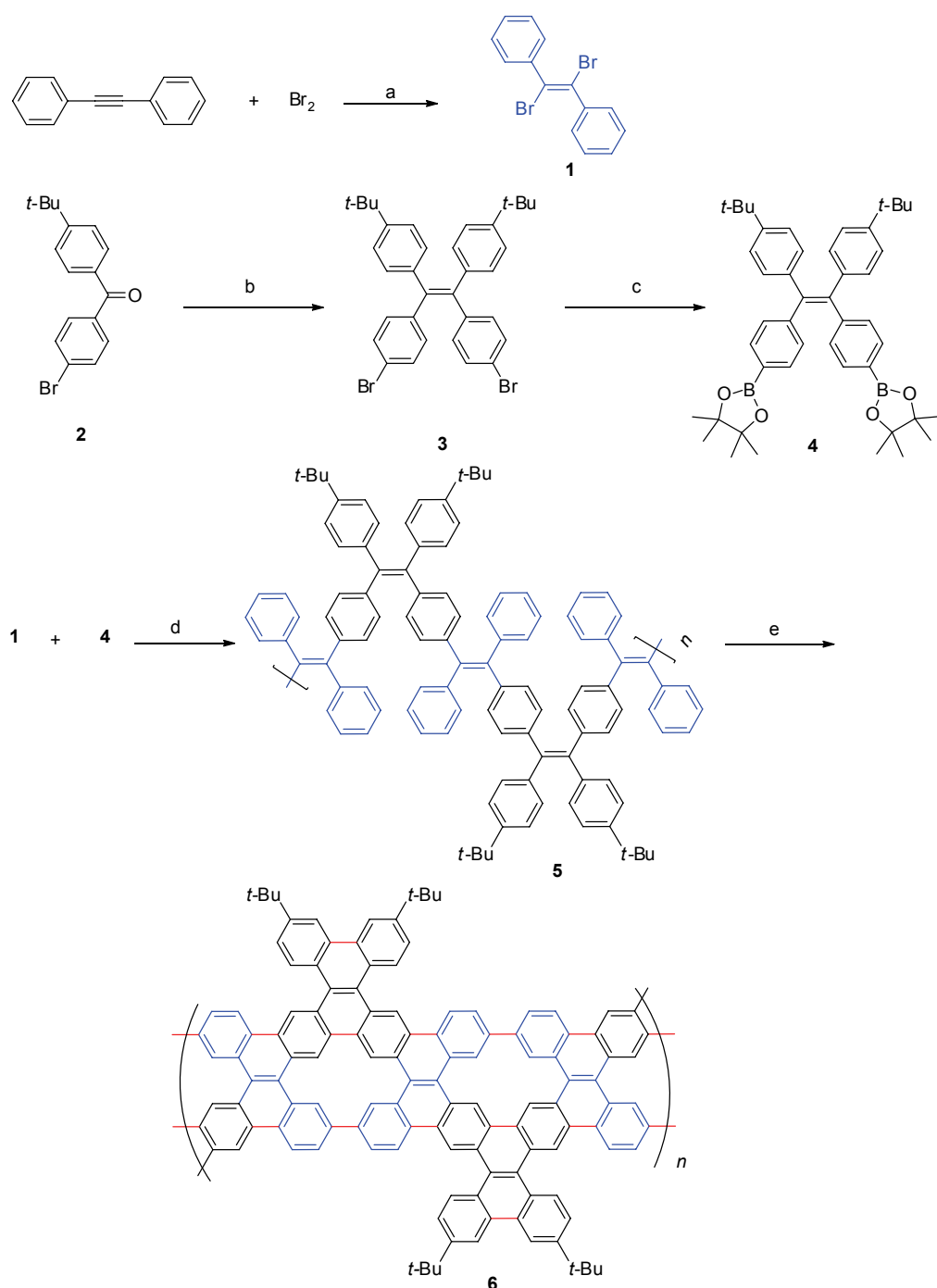
Graphene nanoribbons (6) A solution of polymer **5** (200 mg) in freshly distilled CH₂Cl₂ (150 mL) was purged with argon for 15 min. Then a solution of FeCl₃ (3 g) in 5 mL nitromethane was added dropwise. After 2 h the argon bubbling was stopped and the flask was sealed with a septum. The resulting black solution was stirred at room temperature for 48 h, and then quenched by addition of excess methanol. The precipitate was collected by filtration, and washed with water and methanol. After drying in vacuum, 173.6 mg of **6** was obtained as dark-red powders in 91% yield.

FT IR *v*: 2958, 2926, 2863, 1726, 1605, 1489, 1456, 1393, 1363, 1263, 1179, 1112, 1016, 915, 868, 820, 785, 695. Raman *v*: 1237, 1352, 1603, 2641, 2757 cm⁻¹.

Results and Discussion

Synthesis

The overall synthetic strategy toward GNRs **6** is shown in Scheme 2. These methods of Suzuki coupling and Scholl reactions are effective ways to obtain GNRs as we reported recently.^[32] In order to acquire regular chemical structure, the detailed synthesis steps are listed in the following part. Firstly, the reaction between diphenylacetylene and liquid bromine gave a 85% yield of *trans*-*α,α*-dibromostilbene (monomer **1**). Then, compound **3** was obtained conveniently by McMurry coupling of molecule **2** which was prepared by Friedel-Crafts acylation of *tert*-butylbenzene. Further, the *Z*-isomers of **3** were easily and effectively separated from their dichloromethane/*n*-hexane solutions (*V/V*, 1/5) in good yields by recrystallization (Figure S1, Supporting Information). Subsequently, the corresponding diboronic ester monomer **4** was successfully synthesized using Pd(dppf)₂Cl₂ as a catalyst. The structures of all the starting molecules were confirmed by accurate single-crystal X-ray data and spectroscopic analyses. Their ORTEP drawings are shown in Figure S2, while the crystal data are summarized in Table S1 in the Supporting Information. Having both the dibromide monomer **1** and diboronic ester monomer **4** with defined

Scheme 2 Synthetic routes to GNRs **6**

Reagents and conditions: (a) room temperature (r.t.), 0.5 h; (b) Zn/TiCl₄, THF, reflux; (c) bis(pinacolato)diboron, Pd(dppf)Cl₂, KOAc, 1,4-dioxane, 90 °C, 24 h; (d) Pd(PPh₃)₄, aliquat 336, 2 mol/L K₂CO₃, toluene, reflux, 3 days; (e) FeCl₃, CH₂Cl₂/CH₃NO₂, r.t., 2 days. The inset shows single crystal structures of monomer **1** and monomer **4**, respectively.

configuration in hand, an A_2B_2 -type Suzuki-Miyaura polymerization or namely zipper reaction was performed smoothly in **3 d** to give the kinked PTPE precursor **5** in high yield, which provided a novel access to controllable and highly crowded polyaromatics. Polymer precursor **5** has a weight-average molecular weight of 1.05×10^4 g/mol with a polydispersity index of approximately 1.33 after Soxhlet extraction, according to

size-exclusion chromatography (SEC) analysis against polystyrene standards. Finally, the intramolecular Scholl reaction of the polymer **5** with FeCl₃ as an oxidant in dichloromethane at room temperature for 2 d produced GNRs **6** as a dark-red solid with 91% yield. Precursor **5** and GNRs **6** have the reasonable solubility in common organic solvents, such as THF, toluene, and dichloromethane, owing to the intentional introduction of

tert-butyl groups at their peripheral positions which efficiently hinders their aggregation in solution. In addition, the as-synthesized GNRs showed decomposition temperature >300 °C under nitrogen atmosphere, and no phase transitions were observed prior to the thermal decomposition of the sample (Figures S3 and S4, Supporting Information).

Photophysical and electrochemical properties

To investigate the changes in optical properties resulting from the intramolecular cyclodehydrogenation reaction, the UV/vis spectra of PTPE precursor **5** and GNRs **6** in THF solutions were obtained (Figure 1a). As the planarization of the conjugated backbone leads to the increase of the conjugation length, the GNRs **6** shows a broadened absorption peak at 400 nm and the tail of its absorption spectrum almost extends to 550 nm, which presents a significant red shift comparing to that of the polymer precursor **5**. Figure 1b shows the PL spectra of polymer **5** and nanoribbons **6** in thin solid films. A red-shift of the emission maximum of approximately 130 nm between polymer **5** and conjugated nanoribbons **6** clearly indicated an expanded conjugation. These spectroscopic results, on the other hand, confirm that the FeCl_3 -catalyzed oxidative intramolecular cyclodehydrogenation of PTPE precursor **5** indeed gave rise to the extended π -electron delocalization system **6**. In order to better explain the pronounced fluorescence red shift, cyclic voltammetry (CV) measurements of the as-synthesized compounds were carried out. The CV curves of PTPE precursor **5** and GNRs **6** are shown in Figure S5 in the Supporting Information and the data are summarized in Table 1. The optical band gaps ($E_{\text{g,opt}}$) of **5** and **6** are calculated to be 2.92 and 2.55 eV, which can be determined from the onset wavelength of their UV absorptions (λ_{onset}), respectively. Besides, CV measurements of both polymers in thin films show that polymer **5** has a HOMO/LUMO energy level of $-5.57/-2.65$ eV, and nanoribbons **6** has a HOMO/LUMO level of $-5.52/-2.97$ eV. These experimental data also prove that the conjugation length of PTPE precursor **5** indeed extends after the completion of Scholl reaction.

Table 1 Electrochemical properties of PTPE **5** and GNRs **6**

Compd.	$E_{\text{onset-ox}}^a$ / V	HOMO ^a / eV	λ_{onset}^b / nm	$E_{\text{g,opt}}^b$ /eV	LUMO ^c /eV
PTPE 5	0.82	-5.57	424	2.92	-2.65
GNRs 6	0.77	-5.52	485	2.55	-2.97

^a HOMO = $-e(E_{\text{onset-ox}} - 0.0468) - 4.8$ eV. ^b Calculated from the onset of the UV/vis absorption spectra, $E_{\text{g,opt}} = 1240/\lambda_{\text{onset}}$.

^c Calculated by the equation: LUMO = HOMO + $E_{\text{g,opt}}$.

Raman and FTIR analysis

Raman spectroscopy is a versatile and powerful method to investigate the structural property of carbo-

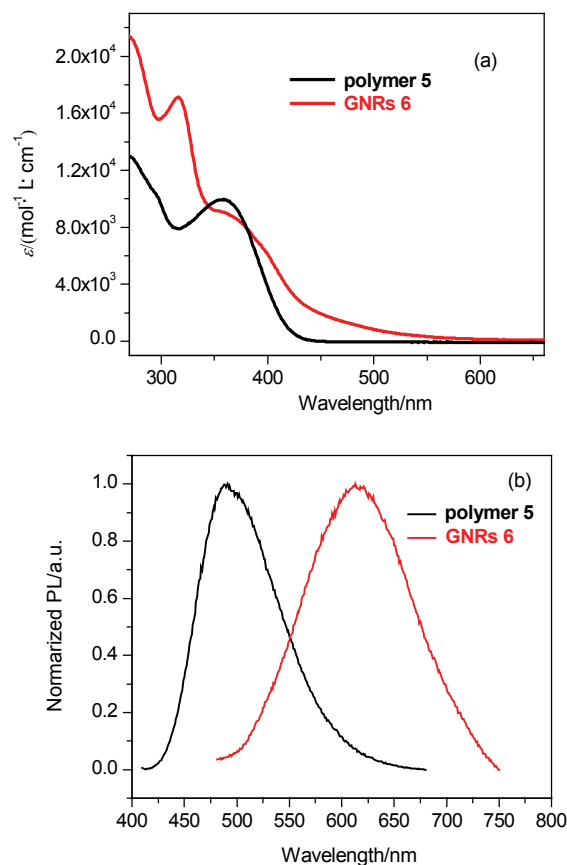


Figure 1 (a) Normalized UV/vis spectra of PTPE precursor **5** and GNRs **6** in THF (1.0×10^{-5} mol/L). (b) Normalized PL spectra of solid thin films of **5** and **6**.

naceous materials. It can provide relevant information about the efficient graphitization of PTPE precursor **5**. Therefore, we used this approach to confirm the high structural quality of the as-prepared GNRs **6** (Figure 2). The powder sample of **6** was measured at a wavelength of 532 nm under laser power of 1 mW. The Raman spectrum shows the first band (D band) located at 1352 cm^{-1} with a shoulder at 1237 cm^{-1} and a second band (G band) located at 1603 cm^{-1} , respectively. These peaks are consistent with those of GNRs synthesized previously by the bottom-up solution approach.^[23,24]

To further evaluate the efficiency of the intramolecular cyclodehydrogenation step, PTPE precursor **5** and GNRs **6**, namely before and after the graphitization, were analyzed by Fourier transform infrared (FTIR) spectroscopy.^[25-27,33] It is clear from the Figure 3 that the out-of-plane C—H deformation bands at 628, 699, 761, and 838 cm^{-1} in the spectrum of precursor **5**, which originate from mono- and di-substituted benzene rings, all disappeared in that of GNRs **6**, corroborating the high efficiency of the intramolecular cyclodehydrogenation. Moreover, the signal triad at 3027, 3057, and 3082 cm^{-1} which is typical for aromatic C—H stretching vibrations was strongly attenuated. These observations clearly supported the successful and efficient conversion of polymer **5** into GNRs **6**.

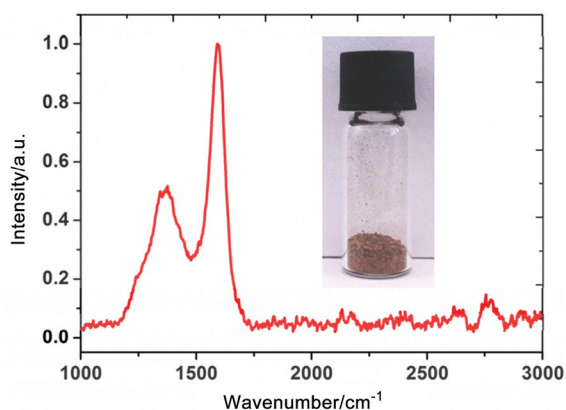


Figure 2 Raman spectrum of the powder of GNRs **6**. Inset: an optical photograph of GNRs **6** powders.

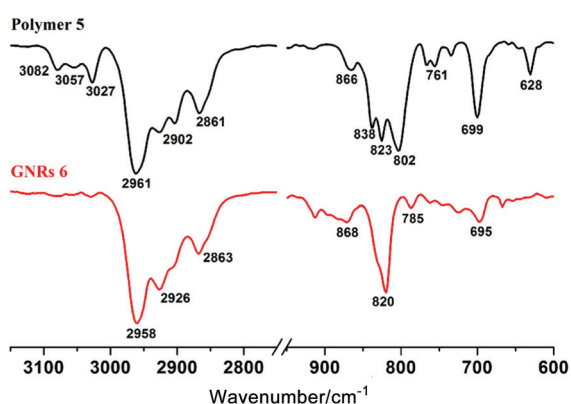


Figure 3 Representative FTIR spectral regions of PTPE precursor **5** and GNRs **6**.

Self-assembly behavior

π -Conjugated polymers always show unique and various self-assembled morphologies due to strong π - π stacking interactions between the aromatic system. Herein, we also investigated the self-assembly behaviors of polymer **5** and GNRs **6**. As shown in Figure 4a, uniform microscale fibers of polymer **5** were observed at the bottom of the beaker after the mixed solvent was slowly evaporated at room temperature. And the SEM image further identified its fibrous microstructures (Figure 4b). In contrast, after drop-casting a toluene solution of GNRs **6** onto a silica substrate followed by slow evaporation of solvent, the large-area sheet-like microstructures with some wrinkles were found by using polarizing microscope (Figure 4c). Furthermore, Figure 4d shows the corresponding STM image obtained at the solid/liquid interface of highly oriented pyrolytic graphite (HOPG)/1-phenyloctane, which provides visualized information on molecular structure. The nanoribbons **6** formed the ordered monolayers and were shown in Figure 4e as the proposed molecular model, the individual elongated nanoribbons with different lengths were aligned parallel to each other, suggesting a face-on arrangement at the basal plane of HOPG as commonly observed for other GNRs.^[22]

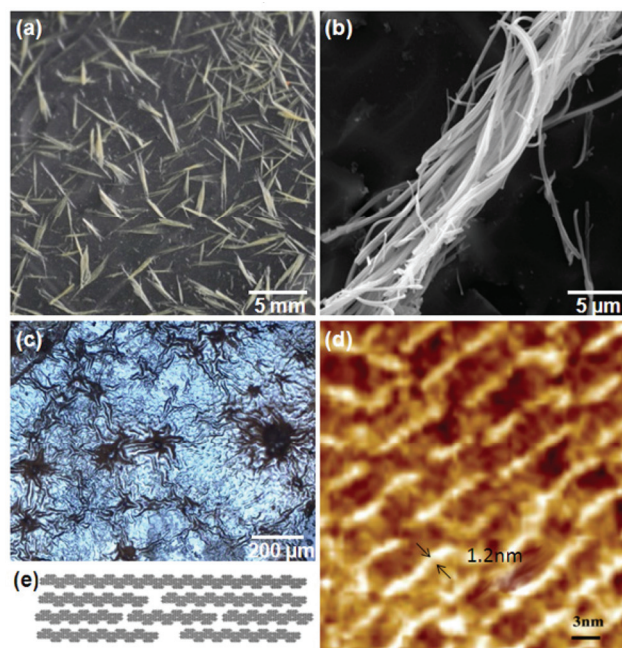


Figure 4 (a) Optical and (b) SEM images of polymer **5** obtained by slow evaporation of its dichloromethane/*n*-hexane mixed solvent. (c) Polarizing microscope image of thin films of GNRs **6**. (d) STM image of **6** at the solid/liquid interface on HOPG. (e) The proposed structure of nanoribbons **6**.

Field-effect transistor application

In particular, GNRs, less than ten nanometers wide, exhibit semiconducting behavior, which allows them to function as active layers in FET devices.^[7,21,34-38] To this end, we fabricated the thin-film FETs from the narrow as-synthesized GNRs **6**. Herein we used ion gel (gelation of an ionic liquid)^[39,40] as the gate dielectric instead of other conventional dielectrics like ZrO₂, HfO₂ or SiO₂.^[41-45] The ion gel with high capacitance is formed at low temperatures. It allows a low voltage operation and hence can effectively diminish the heat generated by the working devices.^[46-48] Most importantly, the top-gated GNRs-based transistors fabricated using ion gel gate dielectrics have been rarely reported.

Figure 5a shows the geometry of the GNRs-based thin film FET devices fabricated by us. Briefly, the semiconducting layer was deposited by spin-coating GNRs **6** solutions (2 mg/mL in toluene) on the cleaned Si/SiO₂ substrate. After thermally annealing the film at 150 °C for 20 min, source and drain electrodes (gold, 50-nm-thick) were vapor-deposited on the GNRs thin film. Subsequently, a kind of ion gel was used as the top gate dielectric (see Supporting Information for the ion gel dielectric formation). The prepared ion solution was drop-cast to cover the surfaces of GNRs film and the drain and source electrodes. Then the transistor channels were covered with a thin aluminum foil (thickness of 0.03 mm) to form the top-gate electrode. The AFM image of the thermally annealed GNRs **6** film shows the crystalline fibrillar intercalating networks, likely the

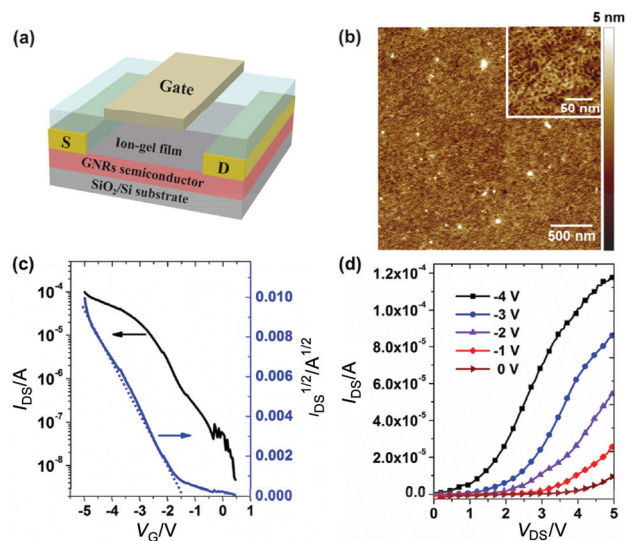


Figure 5 (a) The geometry of top-gated GNRs thin-film FETs fabricated using ion gel gate dielectrics. (b) Tapping-mode AFM height image of GNRs **6** film spin-coated from toluene solutions (2 mg/mL) and annealed at 150 °C. The inset shows a highly magnified image. (c) Transfer and (d) output characteristics of the ion gel gated GNRs **6** devices ($W=L=1000\ \mu\text{m}$) at $V_{\text{DS}}=3\ \text{V}$.

result of the strong intermolecular π - π stacking interactions (Figure 5b and Figure S6). On the other hand, the X-ray diffraction profile of the same GNRs film shows distinct diffraction peak at $2\theta=10.91^\circ$, corresponding to a d-spacing of 8.185 Å (Figure S7, Supporting Information), indicating the existence of the orderly crystalline structures.

Figure 5c and Figure 5d show the typical transfer and output characteristic curves of the above FET devices, respectively. The transfer curve in Figure 5c clearly confirms p-channel FET characteristic with the GNRs **6** layer in devices. The charge carrier mobility was calculated from the saturated regime of the transfer characteristic according to the equation:

$$I_{\text{DS}} = \frac{\mu WC_i}{2L} (V_{\text{G}} - V_{\text{TH}})^2$$

where I_{DS} is the drain current, μ is the field-effect mobility, W is the channel width, L is the channel length, C_i is the specific capacitance of the dielectric, V_{G} is the gate voltage, and V_{TH} is the threshold voltage. From a linear relationship between the $|I_{\text{DS}}|^{1/2}$ versus $|V_{\text{G}}|$ curve obtained at $V_{\text{DS}}=3\ \text{V}$, V_{TH} of the devices is evaluated to be $-1.5\ \text{V}$. The capacitance of ion gel (C_i) is measured to be $20\ \mu\text{F}/\text{cm}^2$. The average mobility was $0.41\ \text{cm}^2\cdot\text{V}^{-1}\cdot\text{s}^{-1}$, which is at least one order of magnitude higher than the reported GNRs-based thin film FET devices,^[49,50] and the on/off current ratio was up to 3×10^4 , indicating a high switching property. Apart from the high performance of the devices involving the obtained GNRs, these devices also show low voltage operation below 5 V, resulting in less energy consumption, which

presents a large advantage in the practical application of the GNRs-based FET devices.

Conclusions

In summary, we have demonstrated that bottom-up solution synthesis of well-defined GNRs **6** from the kinked PTPE precursor **5** is possible through the use of an intramolecular cyclodehydrogenation reaction with FeCl_3 as an oxidant. After the efficient planarization, the GNRs became more conjugated as indicated by UV/vis, PL, and CV results. The chemical identity of GNRs was also validated by Raman and FTIR spectra. The GNRs with more planar conformation can self-assemble to form large-area sheet-like microstructures, indicating their good filming property. Moreover, the top-gated field-effect transistors based on these GNRs films combined with ion gel dielectrics have been successfully developed, exhibiting quite high hole mobility of $0.41\ \text{cm}^2\cdot\text{V}^{-1}\cdot\text{s}^{-1}$ than other GNRs-based thin film FETs, which may create new opportunities for fabricating GNRs-based electronics with mechanically flexible property, high-performance, and low-voltage operation.

Acknowledgement

This work was financially supported by the National Natural Science Foundation of China (21274027 and 20974022) and the Innovation Program of Shanghai Municipal Education Commission (15ZZ02).

References

- [1] Barone, V.; Hod, O.; Scuseria, G. E. *Nano Lett.* **2006**, *6*, 2748.
- [2] Zazyev, O. V. *Acc. Chem. Res.* **2013**, *46*, 2319.
- [3] Ma, L.; Wang, J.; Ding, F. *ChemPhysChem* **2013**, *14*, 47.
- [4] Abbas, A. N.; Liu, G.; Narita, A.; Orosco, M.; Feng, X.; Müllen, K.; Zhou, C. *J. Am. Chem. Soc.* **2014**, *136*, 7555.
- [5] Han, M. Y.; Özyilmaz, B.; Zhang, Y.; Kim, P. *Phys. Rev. Lett.* **2007**, *98*, 206805.
- [6] Bai, J.; Duan, X.; Huang, Y. *Nano Lett.* **2009**, *9*, 2083.
- [7] Li, X.; Wang, X.; Zhang, L.; Lee, S.; Dai, H. *Science* **2008**, *319*, 1229.
- [8] Wang, X.; Ouyang, Y.; Li, X.; Wang, H.; Guo, J.; Dai, H. *Phys. Rev. Lett.* **2008**, *100*, 206803.
- [9] Kosynkin, D. V.; Higginbotham, A. L.; Sinitskii, A.; Lomeda, J. R.; Dimiev, A.; Price, B. K.; Tour, J. M. *Nature* **2009**, *458*, 872.
- [10] Jiao, L.; Zhang, L.; Wang, X.; Diankov, G.; Dai, H. *Nature* **2009**, *458*, 877.
- [11] Sinitskii, A.; Fursina, A. A.; Kosynkin, D. V.; Higginbotham, A. L.; Natelson, D.; Tour, J. M. *Appl. Phys. Lett.* **2009**, *95*, 253108.
- [12] Jiao, L.; Wang, X.; Diankov, G.; Wang, H.; Dai, H. *Nat. Nanotechnol.* **2010**, *5*, 321.
- [13] Chuvilin, A.; Bichoutskaia, E.; Gimenez-Lopez, M. C.; Chamberlain, T. W.; Rance, G. A.; Kuganathan, N.; Biskupek, J.; Kaiser, U.; Khlobystov, A. N. *Nat. Mater.* **2011**, *10*, 687.
- [14] Talyzin, A. V.; Anoshkin, I. V.; Krashennnikov, A. V.; Nieminen, R. M.; Nasibulin, A. G.; Jiang, H.; Kauppinen, E. I. *Nano Lett.* **2011**, *11*, 4352.
- [15] Cai, J.; Ruffieux, P.; Jaafar, R.; Bieri, M.; Braun, T.; Blankenburg, S.; Muoth, M.; Seitsonen, A. P.; Saleh, M.; Feng, X.; Müllen, K.; Fasel, R. *Nature* **2010**, *466*, 470.
- [16] Bronner, C.; Stremlau, S.; Gille, M.; Brauße, F.; Haase, A.; Hecht, S.;

- Tegeder, P. *Angew. Chem., Int. Ed.* **2013**, *52*, 4422.
- [17] Chen, Y.-C.; de Oteyza, D. G.; Pedramrazi, Z.; Chen, C.; Fischer, F. R.; Crommie, M. F. *ACS Nano* **2013**, *7*, 6123.
- [18] Sokolov, A. N.; Yap, F. L.; Liu, N.; Kim, K.; Ci, L.; Johnson, O. B.; Wang, H.; Vosgueritchian, M.; Koh, A. L.; Chen, J.; Park, J.; Bao, Z. *Nat. Commun.* **2013**, *4*, 2402.
- [19] Martin-Fernandez, I.; Wang, D.; Zhang, Y. *Nano Lett.* **2012**, *12*, 6175.
- [20] Kato, T.; Hatakeyama, R. *Nat. Nanotechnol.* **2012**, *7*, 651.
- [21] Liu, N.; Kim, K.; Hsu, P.-C.; Sokolov, A. N.; Yap, F. L.; Yuan, H.; Xie, Y.; Yan, H.; Cui, Y.; Hwang, H. Y.; Bao, Z. *J. Am. Chem. Soc.* **2014**, *136*, 17284.
- [22] Yang, X.; Dou, X.; Rouhanipour, A.; Zhi, L.; Räder, H. J.; Müllen, K. *J. Am. Chem. Soc.* **2008**, *130*, 4216.
- [23] Dössel, L.; Gherghel, L.; Feng, X.; Müllen, K. *Angew. Chem., Int. Ed.* **2011**, *50*, 2540.
- [24] Vo, T. H.; Shekhirev, M.; Kunkel, D. A.; Morton, M. D.; Berglund, E.; Kong, L.; Wilson, P. M.; Dowben, P. A.; Enders, A.; Sinitiskii, A. *Nat. Commun.* **2014**, *5*, 3189.
- [25] Schwab, M. G.; Narita, A.; Hernandez, Y.; Balandina, T.; Mali, K. S.; De Feyter, S.; Feng, X.; Müllen, K. *J. Am. Chem. Soc.* **2012**, *134*, 18169.
- [26] Narita, A.; Feng, X.; Hernandez, Y.; Jensen, S. A.; Bonn, M.; Yang, H.; Verzhbitskiy, I. A.; Casiraghi, C.; Hansen, M. R.; Koch, A. H. R.; Fytas, G.; Ivasenko, O.; Li, B.; Mali, K. S.; Balandina, T.; Mahesh, S.; De Feyter, S.; Müllen, K. *Nat. Chem.* **2014**, *6*, 126.
- [27] Wu, J.; Gherghel, L.; Watson, M. D.; Li, J.; Wang, Z.; Simpson, C. D.; Kolb, U.; Müllen, K. *Macromolecules* **2003**, *36*, 7082.
- [28] Fogel, Y.; Zhi, L.; Rouhanipour, A.; Andrienko, D.; Räder, H. J.; Müllen, K. *Macromolecules* **2009**, *42*, 6878.
- [29] Wang, W.; Lin, T.; Wang, M.; Liu, T.-X.; Ren, L.; Chen, D.; Huang, S. *J. Phys. Chem. B* **2010**, *114*, 5983.
- [30] Zhao, Z.; Lam, J. W. Y.; Tang, B. Z. *J. Mater. Chem.* **2012**, *22*, 23726.
- [31] Ma, J.; Lin, T.; Pan, X.; Wang, W. *Chem. Mater.* **2014**, *26*, 4221.
- [32] Huang, W.; Zhang, H.; Ma, J.; Chen, M.; Zhu, H.; Wang, W. *J. Mater. Chem. C* **2015**, *3*, 6200.
- [33] Centrone, A.; Brambilla, L.; Renouard, T.; Gherghel, L.; Mathis, C.; Müllen, K.; Zerbi, G. *Carbon* **2005**, *43*, 1593.
- [34] Villegas, C. E. P.; Mendonça, P. B.; Rocha, A. R. *Sci. Rep.* **2014**, *4*, 6579.
- [35] Han, M. Y.; Brant, J. C.; Kim, P. *Phys. Rev. Lett.* **2010**, *104*, 056801.
- [36] Zhao, Z.; Li, Z.; Lam, J. W. Y.; Maldonado, J.; Gabriel, R. O.; Liu, Y.; Yuan, W.; Xu, J.; Miao, Q.; Tang, B. Z. *Chem. Commun.* **2011**, *47*, 6924.
- [37] Zhao, Z. J.; Lam, J. W. Y.; Chan, C. Y. K.; Chen, S. M.; Liu, J. Z.; Lu, P.; Rodriguez, M.; Maldonado, J. L.; Ramos-Ortiz, G.; Sung, H. H. Y.; Williams, I. D.; Su, H. M.; Wong, K. S.; Ma, Y. G.; Kwok, H. S.; Qiu, H. Y.; Tang, B. Z. *Adv. Mater.* **2011**, *23*, 5430.
- [38] Chen, L.; Wang, Y. H.; He, B. R.; Nie, H.; Hu, R. R.; Huang, F.; Qin, A. J.; Zhou, X. S.; Zhao, Z. J.; Tang, B. Z. *Angew. Chem., Int. Ed.* **2015**, *54*, 4231.
- [39] Tarabella, G.; Mahvash Mohammadi, F.; Coppede, N.; Barbero, F.; Iannotta, S.; Santato, C.; Cicoira, F. *Chem. Sci.* **2013**, *4*, 1395.
- [40] Fujimoto, T.; Awaga, K. *Phys. Chem. Chem. Phys.* **2013**, *15*, 8983.
- [41] Farmer, D. B.; Chiu, H.-Y.; Lin, Y.-M.; Jenkins, K. A.; Xia, F.; Avouris, P. *Nano Lett.* **2009**, *9*, 4474.
- [42] Liao, L.; Bai, J.; Lin, Y.-C.; Qu, Y.; Huang, Y.; Duan, X. *Adv. Mater.* **2010**, *22*, 1941.
- [43] Lei, T.; Cao, Y.; Fan, Y.; Liu, C.-J.; Yuan, S.-C.; Pei, J. *J. Am. Chem. Soc.* **2011**, *133*, 6099.
- [44] Hu, Y.; Wang, Z.; Zhang, X.; Yang, X.; Li, H.; Gao, X. *Chin. J. Chem.* **2013**, *31*, 1428.
- [45] Cai, Z.; Liu, Z.; Luo, H.; Qi, P.; Zhang, G.; Zhang, D. *Chin. J. Chem.* **2014**, *32*, 788.
- [46] Cho, J. H.; Lee, J.; Xia, Y.; Kim, B.; He, Y.; Renn, M. J.; Lodge, T. P.; Frisbie, C. D. *Nat. Mater.* **2008**, *7*, 900.
- [47] Kim, B. J.; Jang, H.; Lee, S.-K.; Hong, B. H.; Ahn, J.-H.; Cho, J. H. *Nano Lett.* **2010**, *10*, 3464.
- [48] Kaji, Y.; Ogawa, K.; Eguchi, R.; Goto, H.; Sugawara, Y.; Kambe, T.; Akaike, K.; Gohda, S.; Fujiwara, A.; Kubozono, Y. *Org. Electron.* **2011**, *12*, 2076.
- [49] Kim, K. T.; Jung, J. W.; Jo, W. H. *Carbon* **2013**, *63*, 202.
- [50] Gemayel, M. E.; Narita, A.; Dössel, L. F.; Sundaram, R. S.; Kiersnowski, A.; Pisula, W.; Hansen, M. R.; Ferrari, A. C.; Orgiu, E.; Feng, X.; Müllen, K.; Samori, P. *Nanoscale* **2014**, *6*, 6301.

(Zhao, X.)